

<https://doi.org/10.1016/j.scitotenv.2022.155508>

This item is likely protected under Title 17 of the U.S. Copyright Law. Unless on a Creative Commons license, for uses protected by Copyright Law, contact the copyright holder or the author.

Access to this work was provided by the University of Maryland, Baltimore County (UMBC) ScholarWorks@UMBC digital repository on the Maryland Shared Open Access (MD-SOAR) platform.

**Please provide feedback**

Please support the ScholarWorks@UMBC repository by emailing [scholarworks-group@umbc.edu](mailto:scholarworks-group@umbc.edu) and telling us what having access to this work means to you and why it's important to you. Thank you.



# Molar absorption coefficients and acid dissociation constants for fluoroquinolone, sulfonamide, and tetracycline antibiotics of environmental concern

Kiranmayi P. Mangalgi<sup>a,b,\*</sup>, Temitope Ibitoye<sup>a</sup>, Lee Blaney<sup>a</sup>

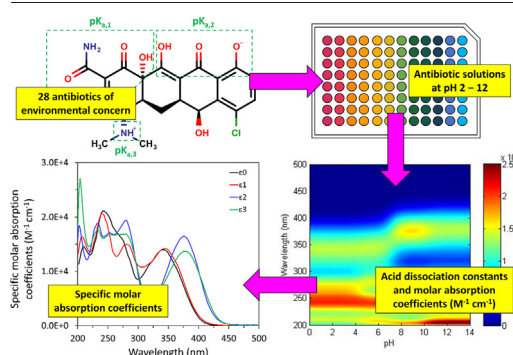
<sup>a</sup> University of Maryland Baltimore County, Department of Chemical, Biochemical, and Environmental Engineering, 1000 Hilltop Circle, Engineering 314, Baltimore, MD 21250, United States of America

<sup>b</sup> Oklahoma State University, Department of Biosystems and Agricultural Engineering, 113 Agricultural Hall, Stillwater, OK 74078, United States of America

## HIGHLIGHTS

- Fast, accurate, precise spectrophotometric method to report  $pK_a$  values of antibiotics
- $pK_a$  values reported for six antibiotics for the first time.
- Database of molar absorption coefficients and  $pK_a$  values for 28 antibiotics
- Novel spectrophotometric justification for  $pK_a$  assignments

## GRAPHICAL ABSTRACT



## ARTICLE INFO

Editor: Shuzhen Zhang

### Keywords:

Antibiotic  
Pharmaceuticals and personal care products  
Molar absorption coefficient  
Acid dissociation constant  
Molar extinction coefficient  
Molar absorptivity

## ABSTRACT

Antibiotics are priority contaminants of emerging concern due to their pseudo-persistence in the environment and contribution to the development of antimicrobial resistance. In solution, antibiotics undergo (de)protonation reactions that affect their UV absorbance and, therefore, photolytic fate in natural and engineered systems. This study employed enhanced spectrophotometric methods to determine the acid dissociation constants (as  $pK_a$  values) and molar absorption coefficients for 12 fluoroquinolone, 9 sulfonamide, and 7 tetracycline antibiotics of environmental relevance. Molar absorption coefficient heatmaps were generated for all 28 antibiotics at 200–500 nm and pH 1.8–12.2. The data in the heatmaps were deconvoluted to calculate  $pK_a$  values and specific molar absorption coefficients at each wavelength. All antibiotics had at least one  $pK_a$  value in the environmentally relevant range of 5.5–8.5, and  $pK_a$  values were reported for methacycline, moxifloxacin, nadifloxacin, rolitetracycline, sulfadoxine, and sulfapyridine for the first time. Deprotonation of the carboxylic acid associated with  $pK_{a,1}$  (5.5–6.7) exerted the strongest effects on the UV absorbance of fluoroquinolones. For tetracyclines, deprotonation of the tertiary amine at  $pK_{a,3}$  (7.8–10.2) was responsible for major shifts in UV absorbance. Although sulfonamides have conserved  $pK_a$  sites, no general trends were observed for the molar absorption coefficients. The structural similarity of fluoroquinolones and tetracyclines supported the potential for a class-based approach to identifying molar absorbance as a function of pH. Overall, the reported  $pK_a$  values and specific molar absorption coefficients will serve as important resources for future studies on antibiotic fate in natural and engineered systems.

\* Corresponding author at: Oklahoma State University, Department of Biosystems and Agricultural Engineering, 113 Agricultural Hall, Stillwater, OK 74078, United States of America.  
E-mail address: [kiranmayi.mangalgi@okstate.edu](mailto:kiranmayi.mangalgi@okstate.edu) (K.P. Mangalgi).

## 1. Introduction

Contaminants of emerging concern (CECs), such as antibiotics, hormones, pesticides, and UV filters, are introduced to the environment from a variety of sources, including wastewater effluent and agricultural runoff (Mangalgi et al., 2015; He et al., 2015; He et al., 2019; Zhang et al., 2019; Barbosa et al., 2018; Hopkins and Blaney, 2016; Van Epps and Blaney, 2016; Mitchelmore et al., 2019). The pseudo-persistence of these biologically-active CECs in the environment has negatively impacted ecological and human health *via* antimicrobial resistance, endocrine disruption, and colony collapse, among other outcomes (Archer et al., 2017; Ben et al., 2019; Zaman et al., 2017; Tosi et al., 2018). The World Health Organization identified antimicrobial resistance as a grand challenge in public health (WHO, 2013), reinforcing the status of antibiotics as priority CECs (Scott et al., 2016). Despite regulatory actions and proposed guidelines in the United States (US) and European Union (US-FDA, 2015; US-EPA, n.d.), global antibiotic consumption increased by approximately 65% between 2000 and 2015 and is expected to expand another 200% by 2030 (Klein et al., 2018). In the US, more than 70% of antibiotic consumption stems from animal feeding operations (PEW, 2018). This situation leads to runoff of antibiotics from fields amended with animal manure (Aga et al., 2016; Fahrenfeld et al., 2014). Furthermore, municipal wastewater treatment plants are not designed to remove CECs, resulting in regular discharge of human-use antibiotics to surface water (He et al., 2019; Guerra et al., 2014; Oberoi et al., 2019). Indeed, a wide array of antibiotics have been detected in the environment at concentrations of 1–1000 ng L<sup>-1</sup> in surface water and 0.5–900 µg kg<sup>-1</sup> in soil (Goel, 2015). To better inform the fate of antibiotics in natural and engineered systems, experimental measurements of key physicochemical properties, such as acid dissociation constants ( $K_a$  values) and molar absorption coefficients, are required.

The majority of environmental studies on antibiotics has been limited to investigation of select molecules, such as ciprofloxacin, chlortetracycline, erythromycin, lincomycin, oxytetracycline, sulfamethoxazole, tylosin, tetracycline, triclosan, and trimethoprim (Dan et al., 2020; Yuan et al., 2019; Shimizu et al., 2013; Shi et al., 2012; Carvalho and Santos, 2016). These compounds are known as “blockbuster” drugs, because they represent the majority of antibiotic sales from specific classes. The chemical properties and environmental fate of other antibiotics, which are being increasingly used in human health and animal agriculture (Van Boeckel et al., 2015), are not always available. Fluoroquinolones, sulfonamides, and tetracyclines tend to be more recalcitrant than other antibiotic classes in both wastewater treatment processes and natural systems (Lu et al., 2018; Feng et al., 2017; Berendsen et al., 2018). For that reason, these antibiotics were prioritized in this study.

Molecules from the three antibiotic classes of concern contain olefins, aromatic rings, and other electron-rich groups that absorb UV light and enable photodegradation. UV processes in drinking water and wastewater treatment plants generally use low-pressure lamps that emit monochromatic light at 254 nm or medium-pressure lamps that employ polychromatic light at 200–400 nm (Bolton and Cotton, 2011). These high-energy light sources enable direct photolysis of antibiotics, although the extent of transformation is low for typical UV doses (Adak et al., 2015). In semi-engineered processes (e.g., lagoons) and surface water, solar radiation emits a broad spectrum of UV and visible light that facilitates both direct and indirect photolysis. In all scenarios, antibiotic photodegradation is a function of the quantum yield (Schwarzenbach et al., 2016) and molar absorption coefficient (McNaught and Wilkinson, 1997). Previous studies have mostly reported molar absorption coefficients for specific experimental conditions, resulting in the incomplete characterization of the UV absorbance spectra of antibiotics as a function of wavelength and solution pH.

Antibiotics contain alcohol (–OH), amine (–NR<sub>3</sub><sup>+</sup>), carboxylic acid (–COOH), and other functional groups that undergo acid dissociation reactions and lead to the occurrence of cationic, zwitterionic, neutral, and anionic species in the aquatic environment. The solution pH and acid dissociation constants control the prevalence of each species. Deprotonation reactions change the electron density and other fundamental

physicochemical properties of antibiotic molecules. Adak et al. (Adak et al., 2015) indicated that pH-dependent molar absorption coefficients and quantum yields rendered the organoarsenical antibiotic, roxarsone, four times more photolabile at neutral pH than at acidic conditions. Similar effects have been reported for oxidation, chlorination, and adsorption reactions (Mangalgi et al., 2015; Adak et al., 2015; Teixidó et al., 2011; Hopkins and Blaney, 2014; Fabiańska et al., 2014; Yang et al., 2011; Goulas et al., 2018). While  $pK_a$  values have been determined for the blockbuster antibiotics, the reported values and their assignment in the antibiotic structure often vary between studies. For example, two  $pK_a$  values were assigned to ciprofloxacin by Völgyi et al. (Völgyi et al., 2007) (i.e., 6.28, 8.26), Snowberger et al. (Snowberger et al., 2016) (i.e., 6.65, 7.31), and the ChemAxon structure-based algorithm (ChemAxon, 2020) (i.e., 5.76, 8.68), but Qiang and Adams (Qiang and Adams, 2004) reported four  $pK_a$  values for ciprofloxacin (i.e., 3.01, 6.14, 8.70, 10.58). Furthermore, the deprotonation sites associated with each  $pK_a$  were not consistent across the literature, as these assignments are often based on predictions stemming from other molecules.

Typically,  $pK_a$  values are determined by potentiometric titration with strong acids or bases (Qiang and Adams, 2004; Babić et al., 2007), but this approach is prone to noise and overfitting due to minor variations in second derivative calculations (Klán and Wirz, 2009). Because electron density at the chromophores is affected by (de)protonation reactions, UV absorbance is a function of solution pH. In fact, absorbance data can be deconvoluted to identify the specific absorbance of the protonated and deprotonated antibiotic molecules, as well as the corresponding  $pK_a$  values (Völgyi et al., 2007; Meloun et al., 2010; Martínez and Dardonville, 2013; Tam and Takács-Novák, 2001). Some authors have reported that this strategy is more accurate than potentiometric titration, because absorbance-based techniques eliminate interferences involved with measurement of solution potential at low and high pH (Berkhout and Aswatha Ram, 2019). Importantly, the wavelengths of UV absorbance peaks are associated with particular moieties in the antibiotic structure, enabling informed assignment of  $pK_a$  values to specific functional groups based on the observed changes in absorbance with solution pH.

The objectives of the present study were to use high-throughput, absorbance-based spectrophotometric methods to calculate (1) the specific molar absorption coefficients for (de)protonated antibiotic molecules and (2) the  $pK_a$  values for 28 antibiotics from three environmentally-relevant classes. In particular, 12 fluoroquinolones, 9 sulfonamides, and 7 tetracyclines that have been detected in wastewater- and agriculture-impacted waters were evaluated using an innovative workflow that employed 96-well microplates and a rigorous data fitting technique. Heatmaps of the molar absorption coefficients were constructed as a function of solution pH and wavelength, and these data were deconvoluted to calculate the specific molar absorption coefficients and  $pK_a$  values for each antibiotic of concern. In addition, differential heatmaps were generated for each antibiotic class to evaluate the role of functional group substitutions on the absorption and acid dissociation properties. Ultimately, these photochemical properties will be useful for future studies of antibiotic photodegradation in both natural and engineered systems.

## 2. Materials and methods

### 2.1. Chemicals and reagents

Chlortetracycline, ciprofloxacin, demeclocycline, difloxacin, doxycycline, enoxacin, enrofloxacin, gatifloxacin, lomefloxacin, marbofloxacin, methacycline, moxifloxacin, nadifloxacin, norfloxacin, ofloxacin, oxytetracycline, rolitetracycline, sarafloxacin, sulfacetamide, sulfadiazine, sulfadoxine, sulfamerazine, sulfamethazine (also known as sulfadimidine), sulfamethizole, sulfamethoxazole, sulfapyridine, sulfathiazole, and tetracycline were procured from Fisher Scientific (Waltham, USA) or Sigma-Aldrich (St. Louis, USA). The purity of all antibiotics was greater than 95%. For all antibiotics, stock solutions were prepared at 400 mg L<sup>-1</sup> in HPLC-grade methanol (Fisher Scientific) and stored at –20 °C. The stock solutions

were diluted with deionized (DI) water (Neu-Ion Systems; Baltimore, USA) to create working solutions with 100 mg L<sup>-1</sup> of individual antibiotics. Fresh working solutions were prepared every three weeks and stored at 4 °C. ACS-grade phosphoric acid and monobasic, dibasic, and tribasic sodium phosphate salts were purchased from Fisher Scientific. Phosphate-buffered solutions (10 mM) were generated at pH 1.8–12.2 and stored at 4 °C for up to two months. The antibiotic working solutions, phosphate buffers, and DI water were mixed at appropriate ratios to generate experimental solutions with 10 mg L<sup>-1</sup> antibiotic (*i.e.*, 18.9–46.7 μM, depending on the particular antibiotic), 9 mM phosphate buffer, and variable pH. The pH of the buffer and experimental solutions was verified by pH meter (Fisher Scientific, Accumet Excel XL15). The final methanol content was 2.5% (v/v) in all experimental solutions. All chemical structures were drawn in Marvin 20.13.0 (ChemAxon, 2020) (ChemAxon, 2020), and the built-in calculator tools were used to predict acid dissociation sites and constants for the antibiotics of concern.

## 2.2. Measurement of UV–visible absorbance spectra

For each antibiotic, absorbance data were collected for the pH 1.8–12.2 range in increments of approximately 1–2 pH units. This scheme resulted in 7–12 absorbance measurements per wavelength. Unlike previously reported spectrophotometric methods, which used the absorbance from a single, fixed wavelength (Boreen et al., 2004), the present study used a wider set of measurements (200–500 nm) to improve the accuracy and precision of the calculated pK<sub>a</sub> values. The UV–visible absorbance spectra were obtained at a 2-nm step size in UV-transparent 96-well microplates (Corning 3635; Corning, USA) using a BioTek Eon microplate reader (Winooski, USA). The temperature control feature of the microplate reader was used to maintain the solutions at 23–25 °C. The plate design involved addition of solutions containing a particular antibiotic across an individual row of the microplate with the solution pH increasing from column A to column H. With this scheme, the absorbance spectra of up to eight antibiotics could be analyzed at 12 pH values within one microplate. A total volume of 300 μL was added to all wells, and the optical pathlength was 0.82 cm (Text S1 in the Supporting Information (SI)). For the tested antibiotic concentrations, the measured absorbance ranged from 0.05 to 1.00 absorbance units. The absorbance spectra of blank solutions, which contained DI water, 2.5% (v/v) methanol, and 9 mM phosphate buffer, were subtracted from the spectra of solutions containing antibiotics to eliminate background signals. All samples were generated in duplicate, and all absorbance measurements were performed in duplicate. The relative difference of absorbance measurements was less than 1.5%.

## 2.3. Determination of pK<sub>a</sub> values and specific molar absorption coefficients

The absorbance data were used to calculate apparent molar absorption coefficients for the antibiotics at pH 1.8–12.2 and 200–500 nm in accordance with the Beer-Lambert law (Eq. (1)).

$$A_{\lambda} = \varepsilon_{\text{app},\lambda,\text{pH}} C \ell \quad (1)$$

In Eq. (1),  $A_{\lambda}$  is the absorbance of the antibiotic at a particular wavelength ( $\lambda$ ),  $\varepsilon_{\text{app},\lambda,\text{pH}}$  is the apparent molar absorption coefficient of the antibiotic at a particular wavelength and solution pH,  $C$  is the molar concentration of the antibiotic, and  $\ell$  is the optical pathlength.

The apparent molar absorption coefficient of the antibiotic comprises contributions from each (de)protonated species and can be described using an additive model. For an antibiotic with  $n$  acid dissociation sites, the pH-dependent apparent molar absorption coefficient at a given wavelength is shown in Eq. (2).

$$\varepsilon_{\text{app},\lambda,\text{pH}} = \sum_{i=0}^n \alpha_{i,\text{pH}} \varepsilon_{i,\lambda} \quad (2)$$

In Eq. (2),  $i$  represents the protonation state of each antibiotic species (*e.g.*, 0 for most protonated, 1 for singly deprotonated, *etc.*),  $\alpha_{i,\text{pH}}$  is the

ionization factor for species  $i$  (*i.e.*, concentration of species  $i$  divided by total antibiotic concentration) at a particular pH, and  $\varepsilon_{i,\lambda}$  is the specific molar absorption coefficient of species  $i$  at wavelength  $\lambda$ . The value of  $\alpha_{i,\text{pH}}$  is a function of the solution pH and the acid dissociation constants of the antibiotic (Eq. (3)).

$$\alpha_{i,\text{pH}} = \frac{\{H^+\}^{-i} \prod_{j=0}^i K_{a,j}}{\sum_{k=0}^n \left( \{H^+\}^{-k} \prod_{j=0}^k K_{a,j} \right)} \quad (3)$$

In Eq. (3),  $K_{a,j}$  is the  $j^{\text{th}}$  acid dissociation constant (note,  $K_{a,0}$  is defined as 1), and  $i$  is the number of antibiotic species generated by  $n$  acid dissociation reactions.

The pK<sub>a</sub> values and specific molar absorption coefficients were simultaneously solved for each wavelength using nonlinear regression tools in Matlab 2017a (MathWorks; Natick, USA). In particular, the  $\varepsilon_{i,\lambda}$  and  $K_a$  (as 10<sup>-pK<sub>a</sub></sup>) parameters in Eqs. (2)–(3) were changed to provide the best fit to the measured apparent molar absorption coefficients. The number of pK<sub>a</sub> values was fixed based on the molecular structure, previous reports for the antibiotic or antibiotic class, and chemical structure-based predictions (ChemAxon, 2020; Qiang and Adams, 2004; Babić et al., 2007). The  $\varepsilon_{i,\lambda}$  and pK<sub>a</sub> values were constrained to be non-negative; furthermore, pK<sub>a</sub> values were constrained to be within 2 pH units of predictions from structure-based algorithms that use site-specific ionization models (Szegedi and Csizmadia, 2004; Szegedi and Csizmadia, 2007). A convergence criterion of 10<sup>-8</sup> was employed, and the system of equations was solved using 10 random starting values for each parameter to avoid local minima. For quality control purposes, model outputs from individual wavelengths in the 200–500 nm range were rejected if the goodness of fit to Eq. (2) was less than 0.85. Rejection generally occurred for wavelengths with low absorbance, and the rejection rate was 23–66%. Higher rejection rates were observed for sulfonamides because of their narrow absorbance domains within the 200–500 nm range. In contrast, tetracyclines demonstrated low rejection due to their broad absorbance of UV and visible light. After accounting for rejection, data from approximately 45 wavelengths (median) were used to calculate each pK<sub>a</sub> value. By fitting a Gaussian distribution to the model outputs for individual wavelengths, the final pK<sub>a</sub> values were determined and then used in conjunction with Eq. (2) to recalculate the specific molar absorption coefficients for each antibiotic at 200–500 nm. All parameters are reported as mean ± standard deviation.

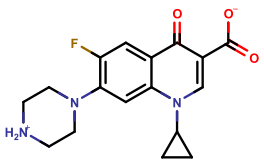
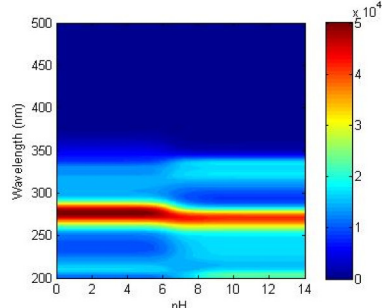
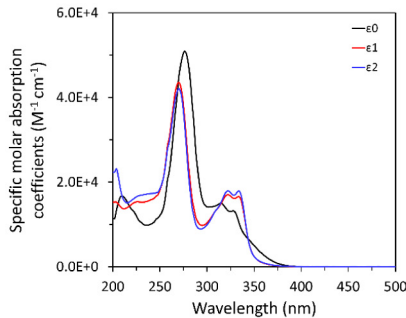
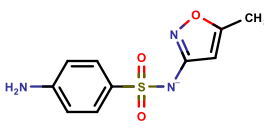
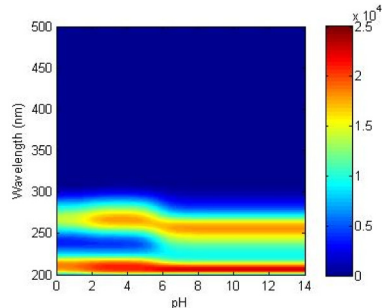
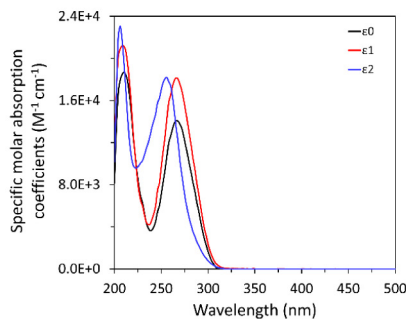
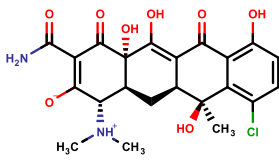
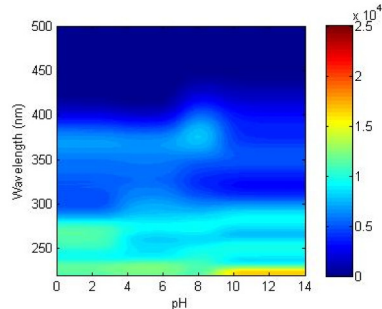
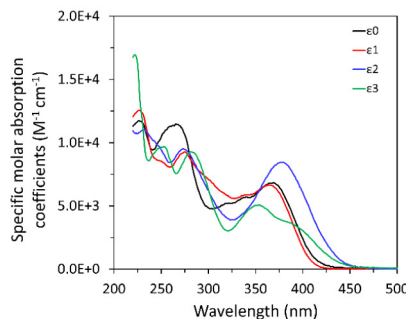
Using the final pK<sub>a</sub> and  $\varepsilon_{i,\lambda}$  values from the regression analyses, heatmaps were generated for each antibiotic in Matlab to depict the apparent molar absorption coefficients at pH 0–14 and 200–500 nm. In addition, the differences in apparent molar absorption coefficients for a given antibiotic with respect to a chosen reference compound (from the same class) were plotted as  $\Delta\varepsilon_{\text{app}}$  heatmaps to highlight the impact of functional group substitutions on the pK<sub>a</sub> and  $\varepsilon_{i,\lambda}$  values. For the fluoroquinolone and tetracycline classes, ciprofloxacin and tetracycline, respectively, were chosen as the reference compounds. Sulfathiazole and sulfadiazine were set as reference compounds for sulfonamide antibiotics containing five- and six-membered rings, respectively; furthermore, sulfacetamide, which does not have a cyclic functional group, was also used to compare the apparent molar absorption coefficients of sulfathiazole and sulfadiazine.

## 3. Results and discussion

The calculated pK<sub>a</sub> values, apparent molar absorption coefficient heatmaps, and specific molar absorption coefficients are reported for all antibiotics in Table 1 and Table S1 in the SI. In general, the individual fluoroquinolone and tetracycline antibiotics exhibited comparable molar absorption coefficients and acid dissociation constants, suggesting minor effects of molecule-specific substitutions on absorbance spectra and deprotonation reactions. In contrast, the individual sulfonamide antibiotics demonstrated greater heterogeneity in the molar absorption coefficients and pK<sub>a</sub> values reported in Table S1. This result stemmed from substitution of

**Table 1**

The chemical structure,  $pK_a$  values, heatmaps of apparent molar absorption coefficients, and specific molar absorption coefficients of three antibiotics evaluated in this study. The location of each  $pK_a$  site is shown in Fig. 1, and the reported values are mean  $\pm$  standard deviation. The reported structure is the dominant species at pH 7.

| Antibiotic   | $pK_a$ value(s)   | Heatmaps of apparent molar absorption coefficients ( $M^{-1} cm^{-1}$ )             | Specific molar absorption coefficients ( $M^{-1} cm^{-1}$ )                           |
|--|---|---|---|
| <b>Ciprofloxacin (Fluoroquinolone class)</b><br>    | $6.40 \pm 0.05$<br><br>$8.06 \pm 0.18$                        |    |    |
| <b>Sulfamethoxazole (Sulfonamide class)</b><br>     | $1.83 \pm 0.19$<br><br>$5.69 \pm 0.04$                        |    |    |
| <b>Chlortetracycline (Tetracycline class)</b><br> | $3.55 \pm 0.13$<br><br>$7.07 \pm 0.08$<br><br>$9.15 \pm 0.14$ |  |  |

different chromophoric groups at the R1 site of the pharmacophore (Fig. 1). The similarity in chemical structures was calculated using Tanimoto coefficients (Willett, 2006). When compared to their respective pharmacophores, the relative standard deviation of the Tanimoto coefficients for antibiotics within each class increased in the following order: tetracyclines (15.9%); fluoroquinolones (21.2%); and, sulfonamides (39.2%). These observations confirm the aforementioned results and justify class-based discussion of acid dissociation constants and molar absorption coefficients.

### 3.1. Acid dissociation constants

For fluoroquinolone antibiotics, the two acid dissociation reactions resulted in the presence of cationic, zwitterionic, and anionic species. The first acid dissociation site was the carboxylic acid group (Fig. 1a), and the corresponding  $pK_{a,1}$  values ranged from  $5.33 (\pm 0.07)$  for ofloxacin to  $6.68 (\pm 0.02)$  for nadifloxacin. The range of  $pK_{a,1}$  values was relatively

small because few chemical substitutions in the fluoroquinolone derivatives occur in the proximity of this site. The second acid dissociation site, which exhibited  $pK_{a,2}$  values of  $7.06 (\pm 0.11)$  for difloxacin to  $8.87 (\pm 0.14)$  for lomefloxacin, was associated with the N13 amine in the piperazine ring. In ciprofloxacin, enoxacin, gatifloxacin, lomefloxacin, norfloxacin, and sarafloxacin, the N13 group is a secondary amine, and the calculated  $pK_{a,2}$  values were  $8.06 (\pm 0.18)$ ,  $8.54 (\pm 0.13)$ ,  $7.30 (\pm 0.13)$ ,  $8.87 (\pm 0.14)$ ,  $7.68 (\pm 0.14)$ , and  $8.60 (\pm 0.04)$ , respectively. For four of the other fluoroquinolones, N13 is a tertiary amine with short alkyl groups that resulted in lower  $pK_{a,2}$  values: difloxacin,  $7.06 (\pm 0.11)$ ; enrofloxacin,  $7.51 (\pm 0.07)$ ; marbofloxacin,  $7.97 (\pm 0.10)$ ; and, ofloxacin,  $7.22 (\pm 0.08)$ . These results agree with findings from Khalili et al. (Khalili et al., 2009), who reported lower  $pK_{a,2}$  values for alkyl substituted piperazines due to steric hindrance during cation solvation which increased acidity. The  $pK_{a,2}$  value of moxifloxacin ( $8.57 \pm 0.05$ ) was not directly comparable to the other fluoroquinolones, because the piperazinyl group was substituted with a



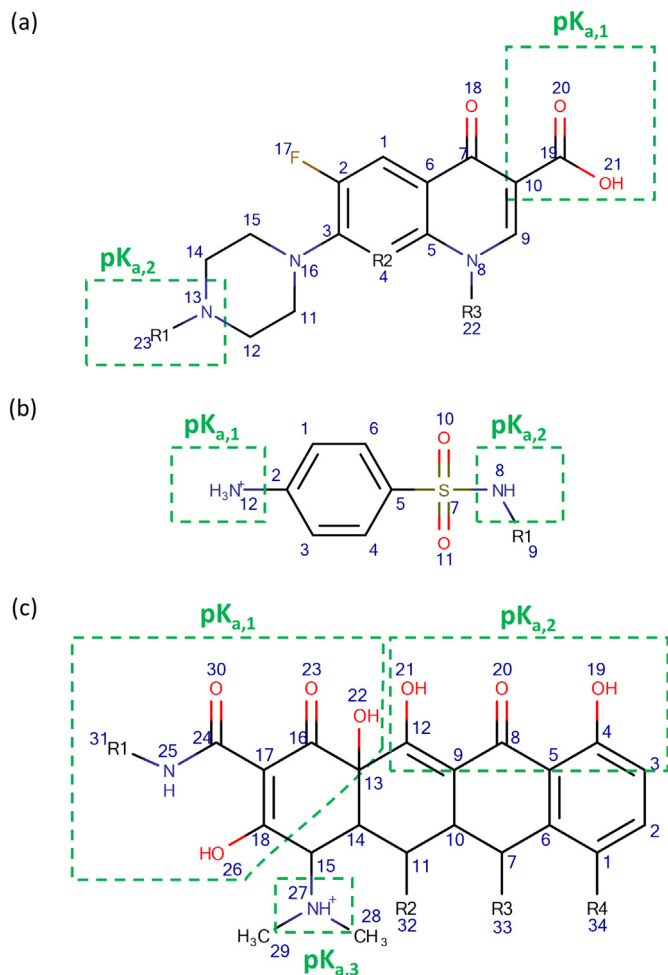


**Fig. 1.** Pharmacophore structures for (a) fluoroquinolones, (b) sulfonamides, and (c) tetracyclines. Note, R1, R2, R3, and R4 represent molecule-specific substitutions, which can be found in Table S1 in the SI. The regions outlined by the dashed lines highlight the acid dissociation sites.

pyrrolopyridine (Table S1 in the SI). In place of the piperazinyl moiety of other fluoroquinolones, nadifloxacin has a piperidinol group that does not undergo acid dissociation; therefore, only one  $pK_a$  value ( $6.68 \pm 0.02$ ) was reported for nadifloxacin.

Two acid dissociation constants were assigned to the sulfonamide antibiotics. The first acid dissociation site was located at the primary amine (N12) of the aniline moiety (Fig. 1b), and the  $pK_{a,1}$  values ranged from  $1.83 (\pm 0.19)$  for sulfamethoxazole to  $2.65 (\pm 0.17)$  for sulfamethizole. The secondary amine (N8) of the sulfonamide group was the second acid dissociation site, with  $pK_{a,2}$  values ranging from  $5.03 (\pm 0.10)$  for sulfacetamide to  $7.81 (\pm 0.14)$  for sulfapyridine. Based on these findings,  $pK_{a,2}$  varied more than  $pK_{a,1}$  due to the different substitutions at the R1 site which caused variable delocalization effects on the N8 group (Milletti et al., 2010). The  $pK_{a,2}$  values of sulfonamides with six-member ring substitutions at R1, namely sulfadiazine ( $6.32 \pm 0.02$ ), sulfadoxine ( $6.43 \pm 0.01$ ), sulfamerazine ( $6.87 \pm 0.06$ ), sulfamethazine ( $6.92 \pm 0.12$ ), and sulfapyridine ( $7.81 \pm 0.14$ ), were generally greater than those of sulfonamides with five-member rings at R1, including sulfamethizole ( $5.47 \pm 0.10$ ) and sulfamethoxazole ( $5.69 \pm 0.04$ ). These results stem from both steric and electronic effects of the substituted moieties. The smaller five-member rings contained nitrogen, sulfur, and/or oxygen atoms that exerted a higher steric hindrance to the secondary amine and decreased the  $pK_{a,2}$  values. One exception was sulfathiazole ( $pK_{a,2} = 7.03 \pm 0.06$ ), which had no substitutions on the five-member ring, unlike sulfamethizole

( $pK_{a,2} = 5.47 \pm 0.10$ ) and sulfamethoxazole ( $pK_{a,2} = 5.69 \pm 0.04$ ) which contain methyl groups. Unlike the other sulfonamides of concern, the R1 substitution of sulfacetamide did not involve a ring. The  $pK_{a,2}$  of sulfacetamide ( $5.03 \pm 0.10$ ) was lower than that of the other sulfonamides due to the electron-withdrawing acetaldehyde group.

Tetracycline antibiotics have more than five theoretical acid dissociation sites (ChemAxon, 2020), but the corresponding species cannot be distinguished due to overlapping resonance structures. As shown in Fig. 1c, the complex speciation characteristics of tetracyclines can be simplified by assigning three macroscopic acid dissociation constants (Hopkins and Blaney, 2014; Qiang and Adams, 2004; Babić et al., 2007) to the following moieties:  $pK_{a,1}$ , keto group at C16, acetamide group at C17, and hydroxyl groups at C13 and C18;  $pK_{a,2}$ , keto group at C8 and hydroxyl groups at C4 and C12; and,  $pK_{a,3}$ , tertiary amine at C15 (Hopkins and Blaney, 2014). The  $pK_{a,1}$  (i.e., 2.30–4.53),  $pK_{a,2}$  (i.e., 5.85–7.18), and  $pK_{a,3}$  (i.e., 7.82–10.20) values did not demonstrate any obvious trends with substitution of electron-donating (e.g., methyl) or -withdrawing (e.g., chloro-, hydroxyl-) groups into the tetracycline pharmacophore. The lack of systematic differences likely stemmed from the high electron density and large number of resonance structures for all tetracyclines. One exception was rolitetracycline, which is chemically similar to tetracycline except for the methylpyrrolidine group present at the R1 site. The addition of methylpyrrolidine notably decreased  $pK_{a,1}$  from 4.34 ( $\pm 0.01$ ) for tetracycline to 3.21 ( $\pm 0.10$ ) for rolitetracycline. A similar effect was observed for  $pK_{a,2}$ , which decreased from  $6.94 \pm 0.07$  for tetracycline to  $5.85 \pm 0.15$  for rolitetracycline.

In general, the  $pK_a$  values measured in this study for blockbuster antibiotics, such as ciprofloxacin, chlortetracycline, and sulfamethoxazole, agreed with experimentally-determined parameters reported in the literature (Table 1, Fig. S5 in the SI). For example, the  $pK_{a,1}$  ( $1.83 \pm 0.19$ ) and  $pK_{a,2}$  ( $5.69 \pm 0.04$ ) of sulfamethoxazole matched the values reported by Boreen et al. (Boreen et al., 2004), who used a single-wavelength spectrophotometric titration to measure  $pK_{a,1}$  ( $1.6 \pm 0.2$ ) and  $pK_{a,2}$  ( $5.7 \pm 0.2$ ). Minor differences were observed for the  $pK_{a,1}$  and  $pK_{a,2}$  values of sulfamethoxazole obtained via potentiometric titration (i.e.,  $1.85 \pm 0.30$  and  $6.08 \pm 0.02$ , respectively) (Qiang and Adams, 2004) and capillary electrophoresis (i.e., 1.83 and 5.57, respectively) (Lin et al., 1997). Larger differences in the  $pK_a$  values were observed for comparisons to chemical structure-based models, as reported in Fig. S5 of the SI for ciprofloxacin and chlortetracycline. It is important to note that the  $pK_a$  values identified in this study tended to the center of the range of previously reported or predicted values; furthermore, the errors on  $pK_a$  values calculated in this study were lower than those determined by other methods. Importantly, experimentally-determined  $pK_a$  values for methacycline, moxifloxacin, nadifloxacin, rolitetracycline, sulfadoxine, and sulfapyridine were reported for the first time.

### 3.2. Molar absorption coefficients

Table 1 and Table S1 show the apparent molar absorption coefficients of antibiotics in the form of heatmaps. In the 200–500 nm range, the antibiotics generally exhibited apparent molar absorption coefficients of  $10^0$ – $10^5 \text{ M}^{-1} \text{ cm}^{-1}$ . The apparent molar absorption coefficients were considered “low” if the magnitude was less than  $10^2 \text{ M}^{-1} \text{ cm}^{-1}$  and “high” if the value was greater than  $10^4 \text{ M}^{-1} \text{ cm}^{-1}$  (Szent-Györgyi and McLaughlin, 1975). The medium-to-high absorbance at 200–350 nm for most antibiotics was attributed to the presence of electron-rich moieties, including aromatic rings, olefins, and atoms with lone pairs of electrons. The molar absorption coefficients varied with substitutions on the antibiotic pharmacophore, and the changes were described as follows: (i) increased (red shift) or decreased (blue shift) wavelength of maximum absorption ( $\lambda_{\text{max}}$ ); and, (ii) increased (hyperchromic shift) or decreased (hypochromic shift) magnitude of absorbance.

The apparent molar absorption coefficients for all antibiotics were greater than  $10^2 \text{ M}^{-1} \text{ cm}^{-1}$  at 254 nm due to the presence of at least one aromatic ring (Table S2 in the SI). This result aligns with the absorbance patterns of individual and fused benzene rings. For example, the maximum

absorbance of benzene occurs at a wavelength of 255 nm due to aromatic pi electron transitions ( $\pi$  to  $\pi^*$ ) and undergoes red shifts upon substitution or fusion to other rings (Taniguchi and Lindsey, 2018). The  $\lambda_{\text{max}}$  for the quinolone moiety in fluoroquinolones was 275 nm (Taniguchi and Lindsey, 2018), but the absorbance extended into the 350–380 nm range due to substitutions (Williams and Fleming, 2007). Similar trends were observed for tetracyclines, which have a fused ring structure that promoted absorbance into the visible range and up to 450 nm. In contrast, the absorbance of sulfonamides was low for wavelengths greater than 320 nm. These observations are reinforced by the apparent molar absorption coefficients reported for 254, 310, and 360 nm in Table S2 of the SI. At pH 7,  $\epsilon_{\text{app}}$ ,  $\epsilon_{\text{app}, 254}$ ,  $\epsilon_{\text{app}, 310}$ , and  $\epsilon_{\text{app}, 360}$  were comparable ( $\sim 10^4 \text{ M}^{-1} \text{ cm}^{-1}$ ) for tetracyclines but differed by up to four orders of magnitude for sulfonamides:  $1\text{--}10 \text{ M}^{-1} \text{ cm}^{-1}$  at 360 nm;  $10^2 \text{ M}^{-1} \text{ cm}^{-1}$  at 310 nm; and,  $10^4 \text{ M}^{-1} \text{ cm}^{-1}$  at 254 nm. For the same conditions, the  $\epsilon_{\text{app}, 254}$  and  $\epsilon_{\text{app}, 310}$  values of fluoroquinolones were comparable ( $\sim 10^4 \text{ M}^{-1} \text{ cm}^{-1}$ ), while  $\epsilon_{\text{app}, 360}$  was lower by an order of magnitude. These observations suggest that, in general, fluoroquinolones and tetracyclines are equally photolabile across the UV and visible light domains compared to sulfonamides.

The presence of lone pairs of electrons on halogen, nitrogen, oxygen, and sulfur atoms in antibiotic molecules also affected the UV absorbance spectra. The transition of non-bonding lone pair electrons ( $n$ ) to antibonding pi ( $\pi^*$ ) and sigma ( $\sigma^*$ ) orbitals requires less energy than the  $\pi$  to  $\pi^*$  transition. The addition of hydroxide to benzene slightly increased the molar absorption coefficient from  $2.1 \times 10^4 \text{ M}^{-1} \text{ cm}^{-1}$  to  $2.3 \times 10^4 \text{ M}^{-1} \text{ cm}^{-1}$  (Taniguchi and Lindsey, 2018). A similar increase in the apparent molar absorption coefficient at 270 nm and pH 7 was observed when hydroxide was added to tetracycline ( $\epsilon_{\text{app}, 270} = 1.4 \times 10^4 \text{ M}^{-1} \text{ cm}^{-1}$ ) to form oxytetracycline ( $\epsilon_{\text{app}, 270} = 1.7 \times 10^4 \text{ M}^{-1} \text{ cm}^{-1}$ ). These impacts were further explored by comparing the apparent and specific molar absorption coefficients for each class of antibiotics, as discussed in the following subsections.

### 3.2.1. Fluoroquinolones

The heatmaps in Table S1 highlights the similarity of the apparent molar absorption coefficients for the fluoroquinolones of concern. The fairly high molar absorption coefficients in the 200–350 nm range were associated with the quinolone moiety, which exhibits absorbance peaks near 220, 265, 305, and 320 nm (Williams and Fleming, 2007). The specific molar absorption coefficient profiles indicated that all fluoroquinolone antibiotics demonstrated the following: a maximum absorbance peak at  $\sim 275$  nm due to the carboxy-substituted quinolone; two minor peaks in the 310–340 nm range associated with the substituted quinolone; and, a peak below 220 nm from the piperazine and quinolone moieties. The primary difference between the fluoroquinolone derivatives was the magnitude of absorbance. For example, the maximum apparent molar absorption coefficients in Table S1 for difloxacin, enrofloxacin, norfloxacin, and sarafloxacin were similar to that of ciprofloxacin ( $\sim 4.5 \times 10^4 \text{ M}^{-1} \text{ cm}^{-1}$ ), but others (e.g., enoxacin, gatifloxacin) were approximately 50% lower ( $\sim 2.1 \times 10^4 \text{ M}^{-1} \text{ cm}^{-1}$ ). The substitution of different functional groups into fluoroquinolones resulted in minor changes to the apparent molar absorption coefficients. For example, the  $\epsilon_{\text{app}, 254}$  values at pH 7 were  $2.01 \times 10^4$ ,  $1.89 \times 10^4$ , and  $1.81 \times 10^4 \text{ M}^{-1} \text{ cm}^{-1}$  for ciprofloxacin, difloxacin, and enrofloxacin, respectively (Table S2 in the SI); note, the secondary amine (N13 in Fig. 1a) on the piperazinyl group in ciprofloxacin is replaced by a tertiary amine in enrofloxacin, and the cyclopropyl ring located at R3 in enrofloxacin is a fluorophenyl group in difloxacin.

Fig. S6 in the SI reports the  $\Delta\epsilon_{\text{app}}$  heatmaps for all fluoroquinolones with respect to ciprofloxacin. For difloxacin and enrofloxacin, few differences were identified at environmentally-relevant wavelengths. These findings indicate that alkylation of the piperazinyl ring and changes in cyclic substitutions at R3 do not exert major impacts on the absorbance of fluoroquinolones. The apparent molar absorption coefficients were also similar for (i) ciprofloxacin and norfloxacin (substitute the cyclopropyl group of ciprofloxacin with an ethyl group) and (ii) difloxacin and sarafloxacin (remove the methyl group from the piperazinyl functionality

of difloxacin). For enoxacin, a nitrogen was substituted at R2, resulting in the loss of the double peak feature in the 310–340 nm region (Table S1); however, the apparent molar absorption coefficients were still comparable to norfloxacin, which was the most structurally similar fluoroquinolone. Careful inspection of the  $\Delta\epsilon_{\text{app}}$  heatmaps indicated higher absorption of ciprofloxacin at 260–280 nm compared to most other fluoroquinolones, resulting in the negative bands observed in Fig. S6 of the SI. In addition, the  $\Delta\epsilon_{\text{app}}$  heatmap for moxifloxacin displayed a strong positive band at 280–310 nm, a result that was likely attributable to the pyrrolopyridine group.

Table 1 and Table S1 shows that the specific molar absorption coefficients for the zwitterionic ( $\epsilon_1$ ) and anionic ( $\epsilon_2$ ) species of each fluoroquinolone were similar to each other but different than the cationic ( $\epsilon_0$ ) species. Deprotonation reactions led to a large hyperchromic red shift for the peaks in the 310–340 nm range and a blue shift for the 275 nm peak. A hyperchromic effect was also observed at 250 nm for the deprotonated fluoroquinolone species. These observations justify the assignment of the acid dissociation constant at pH 5.32–6.68 to the carboxylic acid group, which has a secondary  $\lambda_{\text{max}}$  at 250 nm, instead of the piperazinyl group, which has a  $\lambda_{\text{max}}$  at 210 nm and no remarkable peak at 250 nm (Qiang and Adams, 2004). These results also highlight the important influence of  $\text{pK}_{\text{a},1}$  on the absorbance of fluoroquinolone antibiotics.

### 3.2.2. Sulfonamides

The apparent molar absorption coefficient heatmaps for sulfonamides in Table S1 highlighted a consistent peak at 270 nm from the aniline moiety and additional peaks at 200–250 nm from the substitutions at R1 (Fig. 1b). Large variations in the absorbance trends were observed for 200–250 nm due to the heteroatomic substitutions on the five- and six-member rings at R1, which also led to multiple or broad peaks at 250–350 nm for some sulfonamides. For example, red shifts were observed when methyl and methoxy groups were added to sulfadiazine ( $\lambda_{\text{max}}, \sim 240$  nm) to form sulfamerazine ( $\sim 255$  and  $\sim 280$  nm) and sulfadoxine ( $\sim 260$  nm), respectively. These shifts were further explored using the  $\Delta\epsilon_{\text{app}}$  heatmaps (Fig. S7 of the SI), which showed that the absence of five- and six-member rings on sulfacetamide (compared to sulfathiazole and sulfadoxine, respectively), decreased UV absorbance in the 250 nm band. The differences were less intense for comparisons between sulfonamides with similar ring structures (e.g., for sulfamethizole, sulfamethoxazole, and sulfathiazole with five-member rings; and, for sulfadiazine, sulfadoxine, sulfamerazine, sulfamethazine, and sulfapyridine with six-member rings).

For sulfacetamide, the apparent molar absorption coefficient heatmaps (Table S1) displayed two absorbance bands at 210 nm and 270 nm associated with the amide and aniline groups, respectively. The substitution of aromatic rings at R1 extended the absorbance peaks beyond 300 nm for the other sulfonamides, but the extent of this red shift was highly variable. For example, sulfapyridine exhibited an additional peak ( $\sim 320$  nm) that was not observed for sulfonamides with six-member rings. The absorbance spectrum did not extend beyond 350 nm. In fact, the values for  $\epsilon_{\text{app}, 254}$  at pH 7 ranged from  $1.18 \text{ M}^{-1} \text{ cm}^{-1}$  for sulfadoxine to  $2.03 \times 10^4 \text{ M}^{-1} \text{ cm}^{-1}$  for sulfadiazine, whereas  $\epsilon_{\text{app}, 360}$  was less than  $100 \text{ M}^{-1} \text{ cm}^{-1}$  for all compounds.

For sulfonamides, the specific molar absorption coefficient of the fully protonated species ( $\epsilon_0$ ) at 270 nm was lower than that of the neutral molecule ( $\epsilon_1$ ), and the specific molar absorption coefficient of the anion ( $\epsilon_2$ ) exhibited a large hyperchromic, blue shift relative to  $\epsilon_1$ . While these trends were observed for all sulfonamides, the magnitude of the peak shift was highly variable. For example,  $\epsilon_{1,270}$  for sulfacetamide was comparable to  $\epsilon_{0,270}$  (increase by  $\sim 4.5\%$ ), and the magnitude of  $\epsilon_{2,270}$  was  $\sim 38\%$  greater than  $\epsilon_{1,270}$ . For sulfamethoxazole,  $\epsilon_{1,270}$  was greater than  $\epsilon_{0,270}$  by  $\sim 21\%$ , and  $\epsilon_{2,270}$  was similar to  $\epsilon_{1,270}$ . These findings suggest that a single sulfonamide antibiotic may not be representative of the entire class with respect to absorbance properties. The parameters reported here will, therefore, be useful to future studies of the photochemical fate and treatment of sulfonamides in natural and engineered systems.

### 3.2.3. Tetracyclines

The tetracycline antibiotics demonstrated comparable trends in the apparent molar extinction coefficient heatmaps, a finding that aligns with expectations from the Tanimoto coefficient analysis. The molar absorption coefficients of tetracyclines displayed distinct peaks at  $\sim 260$ – $280$  nm and  $\sim 340$ – $380$  nm due to the fused-ring structure of the pharmacophore. The  $\epsilon_{\text{app}, 254}$  values of chlortetracycline, oxytetracycline, and tetracycline at pH 7 were  $8.50 \times 10^3$ ,  $1.07 \times 10^4$ , and  $1.09 \times 10^4 \text{ M}^{-1} \text{ cm}^{-1}$ , respectively. The chemical structures of chlortetracycline and oxytetracycline differ from that of tetracycline by one substitution, namely the chloro- and hydroxy- groups at the R4 and R2 positions (Fig. 1c), respectively. These results indicate that the pharmacophore is responsible for most of the absorbance of tetracyclines, a finding that was confirmed by the  $\Delta\epsilon_{\text{app}}$  heatmaps (Fig. S8 of the SI), which exhibited fewer features than the fluoroquinolones and sulfonamides. Methacycline, which has a methylene group at C7, showed a positive band in the  $\Delta\epsilon_{\text{app}}$  heatmaps compared to tetracycline, and this finding was also reflected by the higher  $\epsilon_{\text{app}, 254}$  at pH 7 ( $1.64 \times 10^4 \text{ M}^{-1} \text{ cm}^{-1}$ ) (Table S2 in the SI). Compared to chlortetracycline, demeclocycline lacks a methyl group at the R3 position and contains a chloro group at the R4 position (Fig. 1c). These structural differences caused  $\epsilon_{\text{app}, 254}$  to increase from  $8.50 \times 10^3 \text{ M}^{-1} \text{ cm}^{-1}$  (chlortetracycline) to  $1.34 \times 10^4 \text{ M}^{-1} \text{ cm}^{-1}$  (demeclocycline).

For tetracyclines, the acid dissociation site located at the N27 tertiary amine (Fig. 1c) exerted the biggest impact on the specific molar absorption coefficients. All tetracyclines demonstrated minor shifts in the specific molar absorption coefficient from the cation ( $\epsilon_0$ ) to the zwitterion ( $\epsilon_1$ ) and, in most cases, from  $\epsilon_1$  to the monovalent anion ( $\epsilon_2$ ); however, the molar absorption coefficient of the divalent anion ( $\epsilon_3$ ) exhibited dissimilar behavior for all compounds, especially for the peak at  $340$ – $380$  nm, a result that has important implications for solar photolysis. Doxycycline, rolitetracycline, and tetracycline showed major hyperchromic shifts for the peak at  $\sim 350$  nm between  $\epsilon_2$  and  $\epsilon_3$ , with minor changes from  $\epsilon_0$  to  $\epsilon_1$  and  $\epsilon_1$  to  $\epsilon_2$ . Demeclocycline and methacycline were exceptions to this trend, wherein the hyperchromic shift occurred between  $\epsilon_1$  and  $\epsilon_2$ . In contrast, a hypochromic shift in the absorbance at  $350$  nm was identified from  $\epsilon_1$  to  $\epsilon_2$  for chlortetracycline. For oxytetracycline, the peak at  $350$  nm gradually shifted to higher wavelengths ( $370$  nm) from  $\epsilon_0$  to  $\epsilon_3$ . Given the high absorbance of UV-A and UV-B light, these data suggest major impacts of pH on tetracycline photodegradation in natural systems.

## 4. Conclusion

This study improved spectrophotometric methods to determine the acid dissociation constants and molar absorption coefficients of fluoroquinolone, sulfonamide, and tetracycline antibiotics of environmental concern. The use of microplate-based protocols saved time, improved throughput, and decreased resource consumption and waste generation. Experimentally determined acid dissociation constants for methacycline, moxifloxacin, nadifloxacin, rolitetracycline, sulfadoxine, and sulfapyridine were reported for the first time. In general, antibiotics in the fluoroquinolone ( $\text{pK}_{\text{a},1} = 5.33$ – $6.68$ ;  $\text{pK}_{\text{a},2} = 7.22$ – $8.87$ ) and tetracycline ( $\text{pK}_{\text{a},1} = 2.30$ – $4.53$ ;  $\text{pK}_{\text{a},2} = 5.85$ – $7.18$ ;  $\text{pK}_{\text{a},3} = 7.82$ – $10.20$ ) classes exhibited similar acid dissociation constants, but a wide range of  $\text{pK}_{\text{a},2}$  values was measured for sulfonamides ( $\text{pK}_{\text{a},1} = 1.83$ – $2.65$ ;  $\text{pK}_{\text{a},2} = 5.03$ – $7.81$ ). The  $\Delta\epsilon_{\text{app}}$  heatmaps highlighted the high degree of intra-class consistency in absorbance properties for fluoroquinolone and tetracycline antibiotics. The absorbance varied for the cationic, zwitterionic, neutral, and/or anionic forms of each antibiotic, and these differences were captured in the molar absorption coefficient heatmaps and specific molar absorption coefficient profiles reported in Table 1 and Table S1.

As fluoroquinolones and sulfonamides exhibited medium-to-high molar absorption coefficients at  $254$  nm ( $0.78$ – $2.05 \times 10^4 \text{ M}^{-1} \text{ cm}^{-1}$ ), antibiotics from these classes are expected to undergo partial transformation in UV-based treatment systems. Tetracycline antibiotics demonstrated medium-to-high absorbance ( $0.11$ – $1.95 \times 10^4 \text{ M}^{-1} \text{ cm}^{-1}$ ) in the  $254$ – $450$  nm range, indicating that tetracyclines can undergo direct

photolysis in both engineered processes and natural systems exposed to solar irradiation. The extent of photodegradation is dependent on the quantum yield of each antibiotic. Previous studies have shown that fluoroquinolones exhibit quantum yields greater than  $10^{-2} \text{ mol Ein}^{-1}$  for direct photolysis at  $254$  nm (Snowberger et al., 2016; Hopanna et al., 2020; Baeza and Knappe, 2011). Although the magnitude of the apparent molar absorption coefficients for tetracyclines was similar to that for fluoroquinolones, the quantum yields were lower (in the range of  $10^{-3} \text{ mol Ein}^{-1}$ ) for tetracyclines, resulting in slower degradation (Hopanna et al., 2020; Pereira et al., 2007; Liu et al., 2015; Miao et al., 2004; Yang and Carlson, 2003). According to the measured  $\text{pK}_{\text{a}}$  values and molar absorption coefficients, the photodegradation rates of sulfonamide antibiotics are expected to be compound-specific. Ultimately, the  $\text{pK}_{\text{a}}$  values, apparent molar absorption coefficient heatmaps, and specific molar absorption coefficients reported here represent key properties that are needed to better characterize antibiotic speciation and photochemical fate in the aquatic environment.

## CRedit authorship contribution statement

**Kiranmayi P. Mangalgi:** Conceptualization, Methodology, Investigation, Validation, Data curation, Software, Writing – original draft, Visualization. **Temitope Ibitoye:** Investigation, Validation. **Lee Blaney:** Conceptualization, Methodology, Resources, Writing – review & editing, Supervision, Project administration, Funding acquisition.

## Declaration of competing interest

The authors declare that they have no known competing financial interests or personal relationships that could have appeared to influence the work reported in this paper.

## Acknowledgements

We gratefully acknowledge funding from NSF CBET 1510420.

## Appendix A. Supplementary data

Supplementary data to this article can be found online at <https://doi.org/10.1016/j.scitotenv.2022.155508>.

## References

- Adak, A., Mangalgi, K.P., Lee, J., Blaney, L., 2015. UV irradiation and UV-H<sub>2</sub>O<sub>2</sub> advanced oxidation of the roxarsone and nitarsone organoarsenicals. *Water Res.* 70, 74–85.
- Aga, D.S., Lenczewski, M., Snow, D., Muirinen, J., Sallach, J.B., Wallace, J.S., 2016. Challenges in the measurement of antibiotics and in evaluating their impacts in agroecosystems: a critical review. *J. Environ. Qual.* 45 (2), 407–419.
- Archer, E., Petrie, B., Kasprzyk-Hordern, B., Wolfaardt, G.M., 2017. The fate of pharmaceuticals and personal care products (PPCPs), endocrine disrupting contaminants (EDCs), metabolites and illicit drugs in a WWTW and environmental waters. *Chemosphere* 174, 437–446.
- Babić, S., Horvat, A.J., Pavlović, D.M., Kaštelan-Macan, M., 2007. Determination of pK<sub>a</sub> values of active pharmaceutical ingredients. *Trends Anal. Chem.* 26 (11), 1043–1061.
- Baeza, C., Knappe, D.R., 2011. Transformation kinetics of biochemically active compounds in low-pressure UV photolysis and UV/H<sub>2</sub>O<sub>2</sub> advanced oxidation processes. *Water Res.* 45 (15), 4531–4543.
- Barbosa, M.O., Ribeiro, A.R., Ratola, N., Hain, E., Homem, V., Pereira, M.F.R., Blaney, L., Silva, A.M., 2018. Spatial and seasonal occurrence of micropollutants in four portuguese rivers and a case study for fluorescence excitation-emission matrices. *Sci. Total Environ.* 644, 1128–1140.
- Ben, Y., Fu, C., Hu, M., Liu, L., Wong, M.H., Zheng, C., 2019. Human health risk assessment of antibiotic resistance associated with antibiotic residues in the environment: a review. *Environ. Res.* 169, 483–493.
- Berendsen, B., Lahr, J., Nibbeling, C., Jansen, L., Bongers, I., Wipfler, E., Van de Schans, M., 2018. The persistence of a broad range of antibiotics during calve, pig and broiler manure storage. *Chemosphere* 204, 267–276.
- Berkhout, J.H., Aswatha Ram, H., 2019. Recent advancements in spectrophotometric pK<sub>a</sub> determinations: a review. *Indian J. Pharm. Educ. Res.* 53 (4), S475–S480.
- Bolton, J.R., Cotton, C.A., 2011. The Ultraviolet Disinfection Handbook. American Water Works Association.



- Boreen, A.L., Arnold, W.A., McNeill, K., 2004. Photochemical fate of sulfa drugs in the aquatic environment: sulfa drugs containing five-membered heterocyclic groups. *Environ. Sci. Technol.* 38 (14), 3933–3940.
- Carvalho, I.T., Santos, L., 2016. Antibiotics in the aquatic environments: a review of the European scenario. *Environ. Int.* 94, 736–757.
- ChemAxon, 2020. MarvinSuite 20.13.0. 2020 Oct 10.
- Dan, A., Zhang, X., Dai, Y., Chen, C., Yang, Y., 2020. Occurrence and removal of quinolone, tetracycline, and macrolide antibiotics from urban wastewater in constructed wetlands. *J. Clean. Prod.* 252, 119677.
- Fabiańska, A., Białk-Bielińska, A., Stepnowski, P., Stolte, S., Siedlecka, E.M., 2014. Electrochemical degradation of sulfonamides at BDD electrode: kinetics, reaction pathway and eco-toxicity evaluation. *J. Hazard. Mater.* 280, 579–587.
- Fahrenfeld, N., Knowlton, K., Krometis, L.A., Hession, W.C., Xia, K., Lipscomb, E., Libuit, K., Green, B.L., Pruden, A., 2014. Effect of manure application on abundance of antibiotic resistance genes and their attenuation rates in soil: field-scale mass balance approach. *Environ. Sci. Technol.* 48 (5), 2643–2650.
- Feng, L., Casas, M.E., Ottosen, L.D.M., Möller, H.B., Bester, K., 2017. Removal of antibiotics during the anaerobic digestion of pig manure. *Sci. Total Environ.* 603, 219–225.
- Goel, S., 2015. Antibiotics in the environment: a review. In *emerging micro-pollutants in the environment: occurrence*. *Fate Distrib.* 19–42.
- Goulas, A., Sabourin, L., Asghar, F., Haudin, C.S., Benoit, P., Topp, E., 2018. Explaining the accelerated degradation of ciprofloxacin, sulfamethazine, and erythromycin in different soil exposure scenarios by their aqueous extractability. *Environ. Sci. Pollut. Res.* 1–10.
- Guerra, P., Kim, M., Shah, A., Alae, M., Smyth, S., 2014. Occurrence and fate of antibiotic, analgesic/anti-inflammatory, and antifungal compounds in five wastewater treatment processes. *Sci. Total Environ.* 473, 235–243.
- He, K., Soares, A.D., Adejumo, H., McDiarmid, M., Squibb, K., Blaney, L., 2015. Detection of a wide variety of human and veterinary fluoroquinolone antibiotics in municipal wastewater and wastewater-impacted surface water. *J. Pharm. Biomed. Anal.* 106, 136–143.
- He, K., Hain, E., Timm, A., Tarnowski, M., Blaney, L., 2019. Occurrence of antibiotics, estrogenic hormones, and UV-filters in water, sediment, and oyster tissue from the Chesapeake Bay. *Sci. Total Environ.* 650, 3101–3109.
- Hopanna, M., Mangalgi, K., Ibitoye, T., Ocasio, D., Snowberger, S., Blaney, L., 2020. UV-254 transformation of antibiotics in water and wastewater treatment processes. *Contaminants of Emerging Concern in Water and Wastewater*. Elsevier, pp. 239–297.
- Hopkins, Z.R., Blaney, L., 2014. A novel approach to modeling the reaction kinetics of tetracycline antibiotics with aqueous ozone. *Sci. Total Environ.* 468–469, 337–344.
- Hopkins, Z.R., Blaney, L., 2016. An aggregate analysis of personal care products in the environment: identifying the distribution of environmentally-relevant concentrations. *Environ. Int.* 92, 301–316.
- Khalili, F., Henni, A., East, A.L.L., 2009. pKa values of some piperazines at (298, 303, 313, and 323) K. *J. Chem. Eng. Data* 54 (10), 2914–2917.
- Klán, P., Wirz, J., 2009. *Photochemistry of Organic Compounds: From Concepts to Practice*. Wiley.
- Klein, E.Y., Van Boeckel, T.P., Martinez, E.M., Pant, S., Gandra, S., Levin, S.A., Goossens, H., Laxminarayan, R., 2018. Global increase and geographic convergence in antibiotic consumption between 2000 and 2015. *Proc. Natl. Acad. Sci.* 115 (15), E3463–E3470.
- Lin, C.-E., Chang, C.-C., Lin, W.-C., 1997. Migration behavior and separation of sulfonamides in capillary zone electrophoresis III. Citrate buffer as a background electrolyte. *J. Chromatogr. A* 768 (1), 105–112.
- Liu, Y., He, X., Duan, X., Fu, Y., Dionysiou, D.D., 2015. Photochemical degradation of oxytetracycline: influence of pH and role of carbonate radical. *Chem. Eng. J.* 276, 113–121.
- Lu, L., Liu, J., Li, Z., Liu, Z., Guo, J., Xiao, Y., Yang, J., 2018. Occurrence and distribution of tetracycline antibiotics and resistance genes in longshore sediments of the Three Gorges Reservoir, China. *Front. Microbiol.* 9, 1911.
- Mangalgi, K.P., Adak, A., Blaney, L., 2015. Organoarsenicals in poultry litter: detection, fate, and toxicity. *Environ. Int.* 75, 68–80.
- Martínez, C.H.R., Dardonville, C., 2013. Rapid determination of ionization constants (pKa) by UV spectroscopy using 96-well microtiter plates. *ACS Med. Chem. Lett.* 4 (1), 142–145.
- McNaught, A.D., Wilkinson, A., 1997. *Compendium of Chemical Terminology*. 1669. Blackwell Science Oxford.
- Meloun, M., Sýrový, T., Ghasemi, J., 2010. Recent progress in the pKa estimation of druglike molecules by the nonlinear regression of multiwavelength spectrophotometric pH-titration data. *SRX Pharmacol.* 2010.
- Miao, X.-S., Bishay, F., Chen, M., Metcalfe, C.D., 2004. Occurrence of antimicrobials in the final effluents of wastewater treatment plants in Canada. *Environ. Sci. Technol.* 38 (13), 3533–3541.
- Milletti, F., Storch, L., Goracci, L., Bendels, S., Wagner, B., Kansy, M., Cruciani, G., 2010. Extending pKa prediction accuracy: high-throughput pKa measurements to understand pKa modulation of new chemical series. *Eur. J. Med. Chem.* 45 (9), 4270–4279.
- Mitchellmore, C.L., He, K., Gonsior, M., Hain, E., Heyes, A., Clark, C., Younger, R., Schmitt-Kopplin, P., Feerick, A., Conway, A., Blaney, L., 2019. Occurrence and distribution of UV-filters and other anthropogenic contaminants in coastal surface water, sediment, and coral tissue from Hawaii. *Sci. Total Environ.* 670, 398–410.
- Obero, A.S., Jia, Y., Zhang, H., Khanal, S.K., Lu, H., 2019. Insights into the fate and removal of antibiotics in engineered biological treatment systems: a critical review. *Environ. Sci. Technol.* 53 (13), 7234–7264.
- Pereira, V.J., Weinberg, H.S., Linden, K.G., Singer, P.C., 2007. UV degradation kinetics and modeling of pharmaceutical compounds in laboratory grade and surface water via direct and indirect photolysis at 254 nm. *Environ. Sci. Technol.* 41 (5), 1682–1688.
- PEW, 2018. Trends in U.S. Antibiotic Use. <https://www.pewtrusts.org/-/media/assets/2018/08/2018-trends-in-us-antibiotic-use.pdf>. (Accessed 12 December 2018).
- Qiang, Z., Adams, C., 2004. Potentiometric determination of acid dissociation constants (pKa) for human and veterinary antibiotics. *Water Res.* 38 (12), 2874–2890.
- Schwarzenbach, R.P., Gschwend, P.M., Imboden, D.M., 2016. *Environmental Organic Chemistry*. John Wiley & Sons.
- Scott, G.I., Porter, D.E., Norman, R.S., Scott, C.H., Uyaguari-Diaz, M.I., Maruya, K.A., Weisberg, S.B., Fulton, M.H., Wirth, E.F., Moore, J., 2016. Antibiotics as CECs: an overview of the hazards posed by antibiotics and antibiotic resistance. *Front. Mar. Sci.* 3, 24.
- Shi, Y., Gao, L., Li, W., Liu, J., Cai, Y., 2012. Investigation of fluoroquinolones, sulfonamides and macrolides in long-term wastewater irrigation soil in Tianjin, China. *Bull. Environ. Contam. Toxicol.* 89 (4), 857–861.
- Shimizu, A., Takada, H., Koike, T., Takeshita, A., Saha, M., Nakada, N., Murata, A., Suzuki, T., Suzuki, S., Chiem, N.H., 2013. Ubiquitous occurrence of sulfonamides in tropical Asian waters. *Sci. Total Environ.* 452, 108–115.
- Snowberger, S., Adejumo, H., He, K., Mangalgi, K.P., Hopanna, M., Soares, A.D., Blaney, L., 2016. Direct photolysis of fluoroquinolone antibiotics at 253.7 nm: specific reaction kinetics and formation of equally potent fluoroquinolone antibiotics. *Environ. Sci. Technol.* 50 (17), 9533–9542.
- Szegedi, J., Cszizmadia, F., 2004. Prediction of distribution coefficient using microconstants. Abstracts of Papers of the American Chemical Society, 2004. American Chemical Society, 1155 16TH ST, NW, Washington, DC 20036 USA.
- Szegedi, J., Cszizmadia, F., 2007. Method for calculating the pKa values of small and large molecules. Abstracts of Papers of the American Chemical Society, 2007. American Chemical Society, 1155 16TH ST, NW, Washington, DC 20036 USA.
- Szent-Györgyi, A., McLaughlin, J.A., 1975. Interaction of glyoxal and methylglyoxal with biogenic amines. *Proc. Natl. Acad. Sci.* 72 (4), 1610–1611.
- Tam, K.Y., Takács-Novák, K., 2001. Multi-wavelength spectrophotometric determination of acid dissociation constants: a validation study. *Anal. Chim. Acta* 434 (1), 157–167.
- Taniguchi, M., Lindsey, J.S., 2018. Database of absorption and fluorescence spectra of > 300 common compounds for use in photochem CAD. *Photochem. Photobiol.* 94 (2), 290–327.
- Teixidó, M., Pignatello, J.J., Beltrán, J.L., Granados, M., Peccia, J., 2011. Speciation of the ionizable antibiotic sulfamethazine on black carbon (biochar). *Environ. Sci. Technol.* 45 (23), 10020–10027.
- Tosi, S., Costa, C., Vesco, U., Quaglia, G., Guido, G., 2018. A 3-year survey of Italian honey bee-collected pollen reveals widespread contamination by agricultural pesticides. *Sci. Total Environ.* 615, 208–218.
- US-EPA, Contaminant Candidate List 4. <https://www.epa.gov/ccl/chemical-contaminants-ccl-4>. (Accessed 12 October 2018).
- US-FDA, 2015. Veterinary Feed Directive: 80 FR 31707. 80 FR 31707. US-FDA.
- Van Boeckel, T.P., Brower, C., Gilbert, M., Grenfell, B.T., Levin, S.A., Robinson, T.P., Teillant, A., Laxminarayan, R., 2015. Global trends in antimicrobial use in food animals. *Proc. Natl. Acad. Sci.* 112 (18), 5649–5654.
- Van Epps, A., Blaney, L., 2016. Antibiotic residues in animal waste: occurrence and degradation in conventional agricultural waste management practices. *Curr. Pollut. Rep.* 2 (3), 135–155.
- Völgyi, G., Ruiz, R., Box, K., Comer, J., Bosch, E., Takács-Novák, K., 2007. Potentiometric and spectrophotometric pKa determination of water-insoluble compounds: validation study in a new cosolvent system. *Anal. Chim. Acta* 583 (2), 418–428.
- WHO, 2013. *Critically Important Antimicrobials for Human Medicine*. 4th revision.
- Willett, P., 2006. Similarity-based virtual screening using 2D fingerprints. *Drug Discov. Today* 11 (23), 1046–1053.
- Williams, D.H., Fleming, I., 2007. *Spectroscopic methods in organic chemistry*, 6th ed. McGraw-Hill Education, London, p. 304.
- Yang, S., Carlson, K., 2003. Evolution of antibiotic occurrence in a river through pristine, urban and agricultural landscapes. *Water Res.* 37 (19), 4645–4656.
- Yang, S.-F., Lin, C.-F., Lin, A.Y.-C., Hong, P.-K.A., 2011. Sorption and biodegradation of sulfonamide antibiotics by activated sludge: experimental assessment using batch data obtained under aerobic conditions. *Water Res.* 45 (11), 3389–3397.
- Yuan, S.-F., Liu, Z.-H., Yin, H., Dang, Z., Wu, P.-X., Zhu, N.-W., Lin, Z., 2019. Trace determination of sulfonamide antibiotics and their acetylated metabolites via SPE-LC-MS/MS in wastewater and insights from their occurrence in a municipal wastewater treatment plant. *Sci. Total Environ.* 653, 815–821.
- Zaman, S.B., Hussain, M.A., Nye, R., Mehta, V., Mamun, K.T., Hossain, N., 2017. A review on antibiotic resistance: alarm bells are ringing. *Cureus* 9, (6).
- Zhang, Y., Duan, L., Wang, B., Du, Y., Cagnetta, G., Huang, J., Blaney, L., Yu, G., 2019. Wastewater-based epidemiology in Beijing, China: prevalence of antibiotic use in flu season and association of pharmaceuticals and personal care products with socioeconomic characteristics. *Environ. Int.* 125, 152–160.